Supplemental Information

Modulating Reactivity and Stability of Metallic Lithium *via* Atomic Doping

Ke Lu,[a] Haiping Xu,[a] Haiying He,[b] Siyuan Gao,[a] Xun Li,[a] Chong Zheng,[a] Tao Xu*[a] and Yingwen Cheng*[a]

[a] Department of Chemistry and Biochemistry, Northern Illinois University, DeKalb, Illinois, 60115, United States.

*E-mail: ycheng@niu.edu (Y.C.) and txu@niu.edu (T.X.)

[b] Department of Physics and Astronomy, Valparaiso University, Valparaiso, Indiana, 46383, United States.

Methods

Doping of Li metal: The doping was performed inside an argon-filled glovebox where the oxygen and moisture levels were both < 0.5 ppm. Typically, 2.0 g Li metal (99.9%, Sigma-Aldrich) was added to a nickel crucible (10 ml), which was slowly heated to 220°C using a heating mantle to melt Li. Afterwards appropriate amount of Ag wires (99.9%, Alfa-Aesar) was added and they generally dissolve in molten Li quickly. The mixture was maintained at 220°C for 2 hours to ensure complete solvation of Ag in Li. The molten Li was then quenched to room temperature and the doped Li was obtained. The surface layers of each doped Li lump was carefully removed using a razor blade prior to pressing into foils with the thickness of 400, 80 or 30 μm using a rolling press. These foils were cut into 16 mm discs for investigation of their properties and electrochemical behavior. The undoped Li electrodes were prepared using the identical procedure without addition of dopants to ensure fair comparison.

Materials characterization: XRD measurements were carried out on a Rigaku MiniFlex X-ray diffractometer operating at 30 kV and 15 mA using Cu Kα radiation (λ=0.15405 nm). SEM images were collected using either a Tescan Vega II microscope or a field-emission Hitachi S-4700-II SEM; and EDX spectra were collected using an INCAx-act Analytical EDS detector (Oxford Instruments). The electrodes for analysis were washed repeatedly inside a glovebox prior to analysis. The XPS spectra were collected using a Kratos AXIS Ultra DLD spectrometer, and the acquired binding energies were calibrated by assigning the C 1s peak at 284.5 eV.

Computation methods: The structures, energetics and electronic structures of pristine Li bulk, Ag-doped Li bulk, pristine Li (100) surface and Ag-doped Li (100) surface were calculated based on the density functional theory (DFT) using the VASP program.[1] The PBE exchange-correlation functional[2] within the Generalized Gradient Approximation (GGA) were adopted for all calculations. The projector augmented wave (PAW) method and plane wave basis sets were used with energy cutoffs of 400 eV. The total energy was converged to 10^{-5} eV for each electronic step using self-consistent field method and the criterion for the force on each atom was set to 0.03 eV/Å. The pristine and doped Li (100) surfaces were modelled by 4×4 periodic slabs with a thickness of 6 Li atomic layers and a vacuum layer of 15 Å placed along the *z* direction. The bottom two Li layers were kept fixed at the bulk values. The surface Brillouin zone was

sampled with a 5×5×1 Monkhorst-Pack *k*-point mesh. Bader charge analysis was conducted to analyze charge populations.[3] The binding energy of a Li adatom was calculated as $E_b = E^{adatom}_{tot} - E^{surf}_{tot} - \mu_{Li}$, where E^{adatom}_{tot} and E^{surf}_{tot} are the calculated total energies of the Ag-doped or pristine Li (100) surface with and without the Li adatom, respectively; μ_{Li} is the chemical potential of Li, which is set to the atomic energy of a Li atom.

Electrochemical measurements: Electrochemical studied were performed using type 2025 coin cells. Cyclic voltammograms were recorded using a CH Instruments potentiostat. Battery cycling behavior was evaluated using Neware CT-4008 battery analyzers. Electrochemical impedance spectra were acquired at room temperature with a frequency range of 0.02 Hz to 100 kHz. The symmetric cells were assembled using Li metal anodes of identical composition and the electrolyte was 1.0M $LiPF_6$ in ethylene carbonate/diethyl carbonate (EC/DEC, 1:1 vol). The electrolyte volumes were 70 µl unless otherwise noted. The NCM 811 electrodes (~ 9.12 mg cm^{-2}) were supplied by the Cell Analysis, Modeling, and Prototyping Facility at Argonne National Laboratory. The electrodes were punched into 16 mm discs and vacuum dried at 75°C overnight before use. The batteries were cycled first at 0.1C for 3 cycles and then at 1.0 C for 200 cycles, with a voltage window of 2.7 to 4.3 V. A combination of constant current and constant voltage charging protocol was used, and when the charging voltage reached 4.3V, the battery was hold at 4.3 V until the charging current decreased to the value equivalent to 0.1C (1C = 1.5 mA/cm^2).

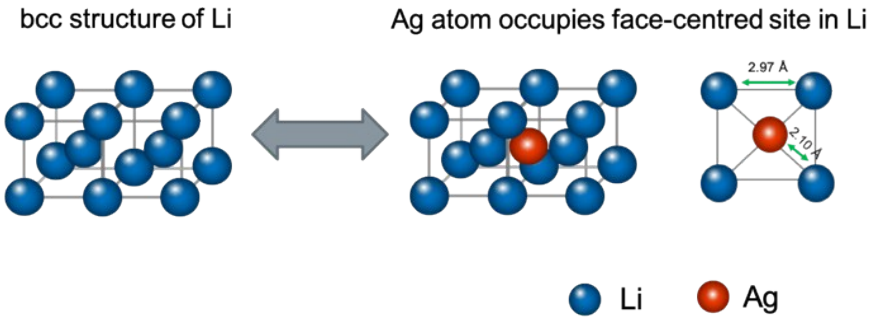

The rational of positioning Ag atoms at face-centered sites in Li crystal structure

A major evidence is based on the correlation of enhanced (200) peak with the systematically absent reflection rules due to lattice type. According to the general X-ray diffraction theory, the rules for reflections of facets with Miller indices (hkl) to be observed are such that:

1. For body centred cubic (BCC) type, the rule is h+k+l=2n (an even number)
2. For face centred cubic (FCC) type, the rule is that h, k and l are either all odd or all even numbers.

We focus on BCC and FCC because pristine Li is in BCC crystal structure, and if we position Ag atoms at face centered sites then we have FCC crystal structure (see the above illustrative picture). We obtain the following results when applying the selection rules to the major Miller indices of BCC and FCC structures:

Miller indices (hkl)	BCC (h+k+l)	FCC
(100)	1, inactive	inactive
(110)	2, active	inactive
(111)	3, inactive	all odd numbers, active
(200)	**2, active**	**all even numbers, active**
(211)	4, active	inactive
(220)	4, active	all even numbers active

These results suggest that the reflection of (200) facet in active in both Ag doped Li crystals (FCC) and pristine Li crystals (BCC), and therefore exhibits enhanced intensity.

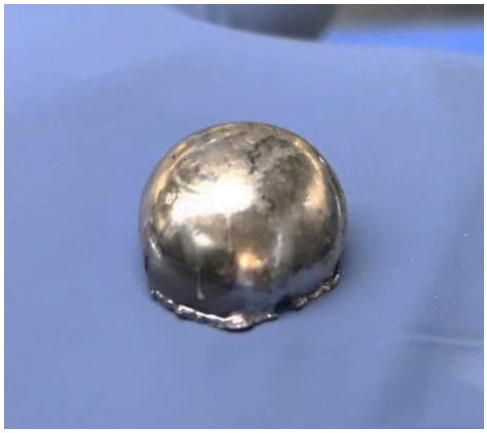

Figure S 1: Photograph of as-prepared Ag-doped Li metal lump.

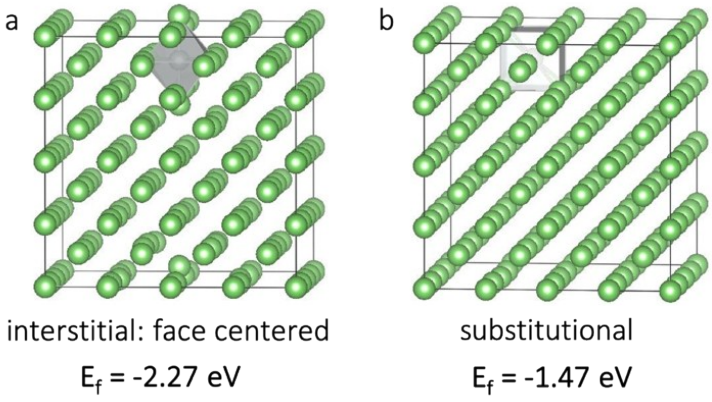

Figure S 2: DFT calculations of the formation energy of positioning Ag atoms at interstitial vs. substitutional sites in Li crystals. The formation energy of defects was calculated as $E_f = E^{defect}_{tot} - E^{pristine}_{tot} - \sum_i n_i \mu_i$, where E^{defect}_{tot} and $E^{pristine}_{tot}$ are the calculated total energies of Ag-doped and pristine Li bulk materials, respectively, i stands for Ag or Li and μ_i the chemical potential of the element based on its atomic energy.

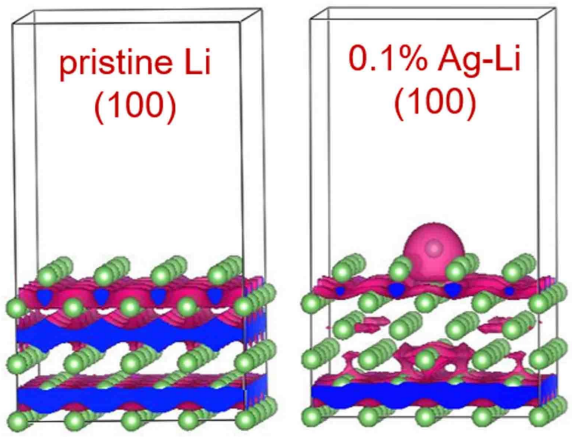

Figure S 3: DFT results of charge distribution (not including inner shell electrons) in pristine and Ag-doped Li (100) surface with the isosurface value set to = 0.0080 e/Å^3.

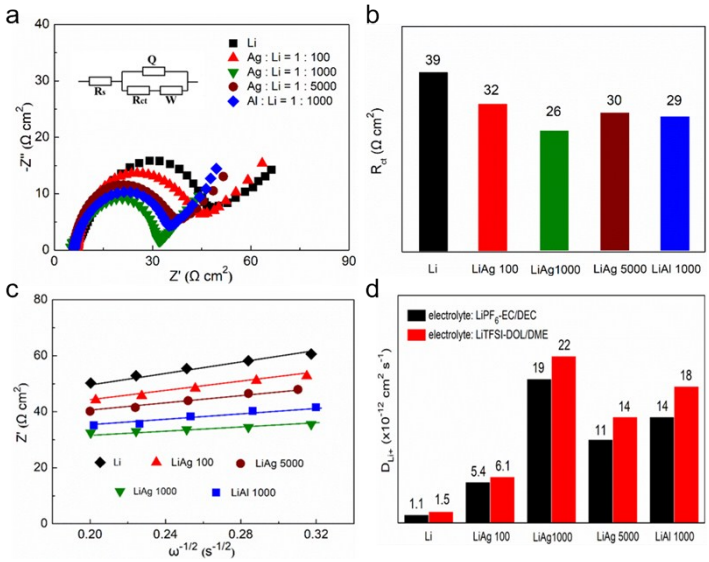

Figure S 4: a) Nyquist plot of coin cells assembled with symmetric Li electrodes with varied doping in carbonate electrolyte; the inset shows the equivalent circuit for modeling Rs: electrolyte resistance; Q: contant phase elements; R_{ct}: charge transfer resistance at Li surface; Z_w: Warburg impedance; and comparison of b) charge-transfer resistance and c) the low-frequency relationships between Z_{re} and $\omega^{-1/2}$ of different electrodes; d) comparison of Li-ion diffusion coefficient in ether and carbonate electrolytes.

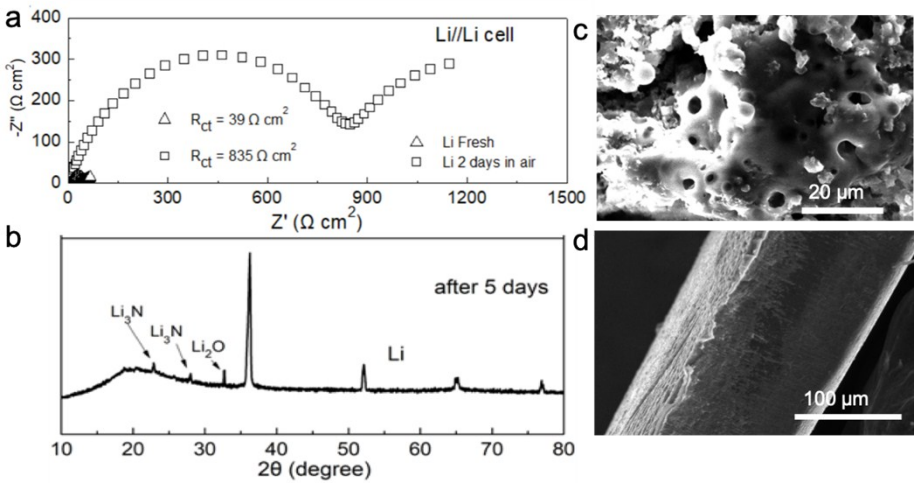

Figure S 5: Characterizations of pristine Li electrodes after different days of exposure in dry air: a) Nyquist plot of symmetric coin cells; b) XRD pattern and c-d) SEM images.

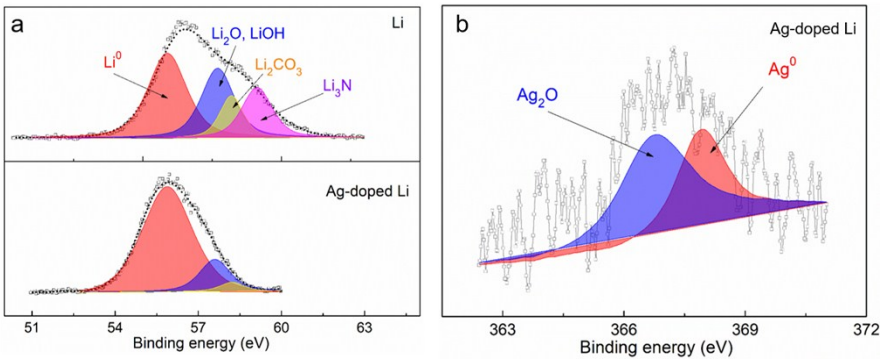

Figure S 6: a) comparison of Li 1s XPS spectra for Ag-doped Li and undoped Li after exposure in dry air; b) Ag 3d XPS spectra for Ag-doped Li after exposure in dry-air.

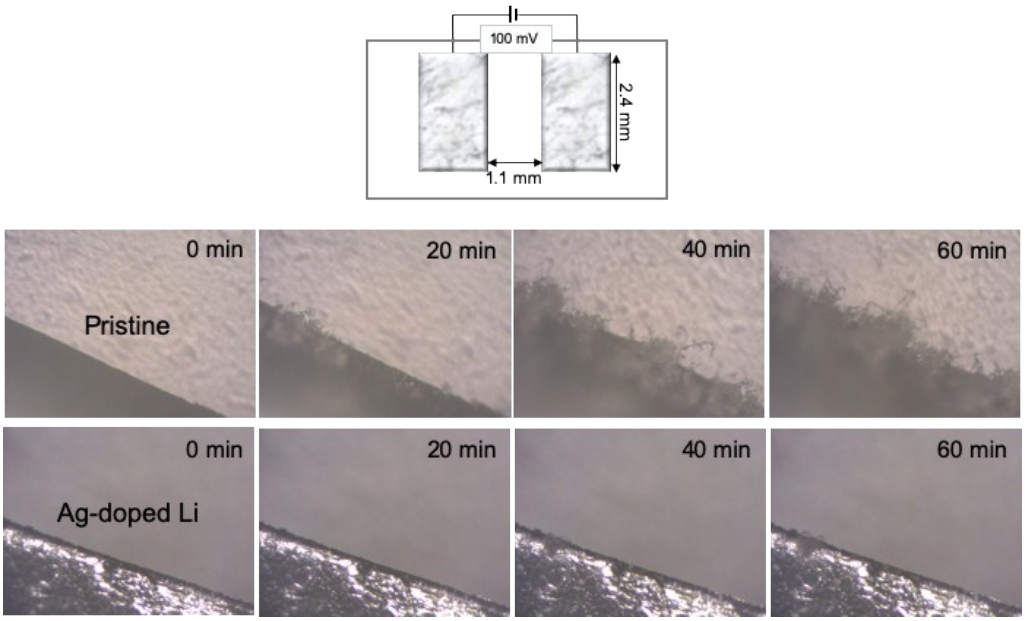

Figure S 7: Schematic illustration for the optical cell built to visualize the Li-electrolyte interface and additional photographs acquired during Li deposition on pristine and Ag doped Li electrodes.

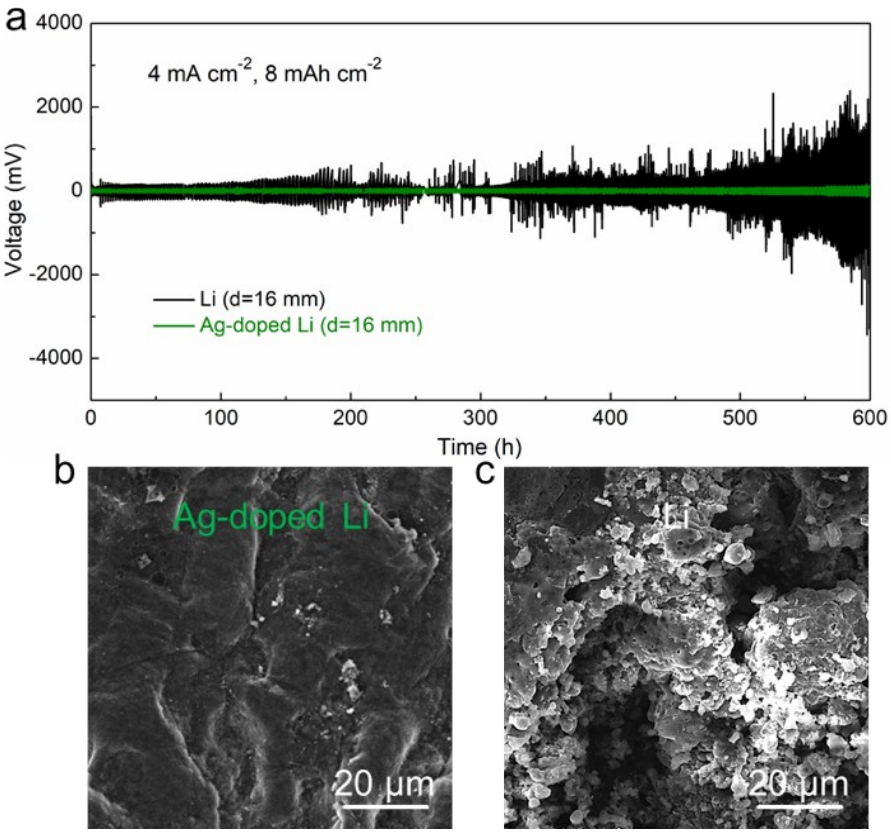

Figure S 8: (a) Voltage profiles of symmetric coin cells tested at 4 mA cm^{-2} for a capacity of 8 mAh cm^{-2} per cycle. Post-mortem SEM images of (b) Ag-doped Li and (c) pristine Li electrodes after cycling test.

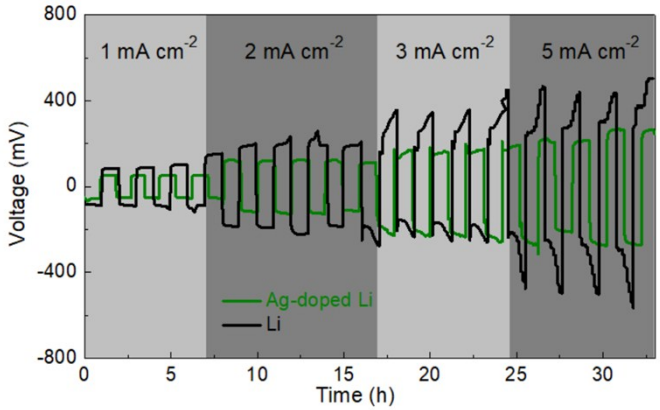

Figure S 9: Comparison of overpotentials for symmetric coin cells assembled with Ag-doped Li and undoped Li at different current densities.

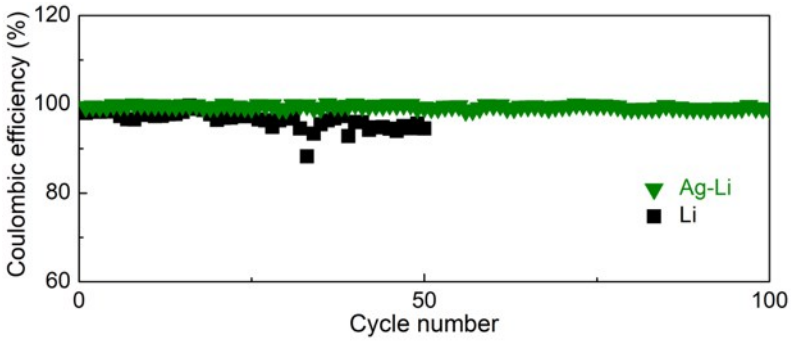

Figure S 10: Coulombic efficiency of full cell Li metal batteries assembled with ~30 µm doped and pristine Li electrodes.

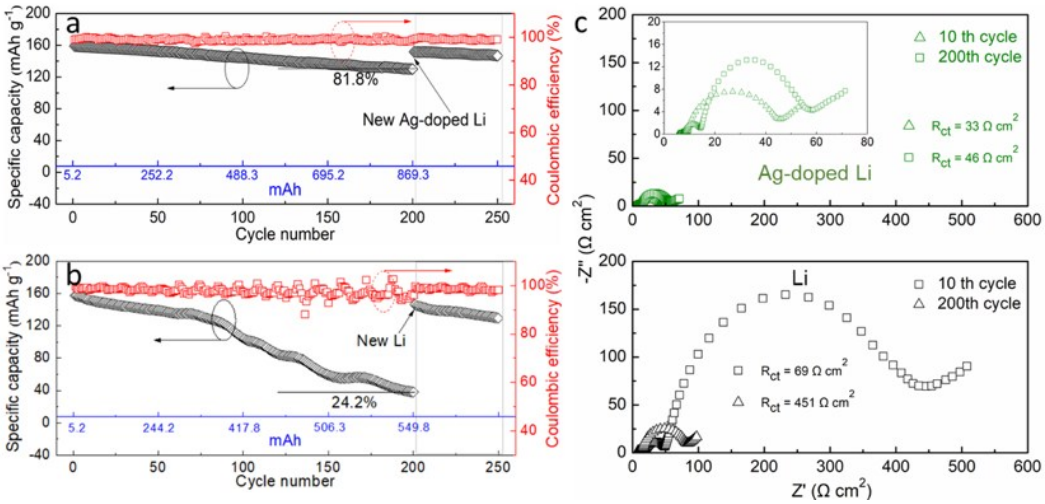

Figure S 11: Cycling stability of full cell Li metal batteries assembled with ~400 µm (a) doped or (b) pristine Li foils. This should be considered as conventional testing condition and the results are directly comparable with literature results. (c) Nyquist plot acquired at different stages of cycling.

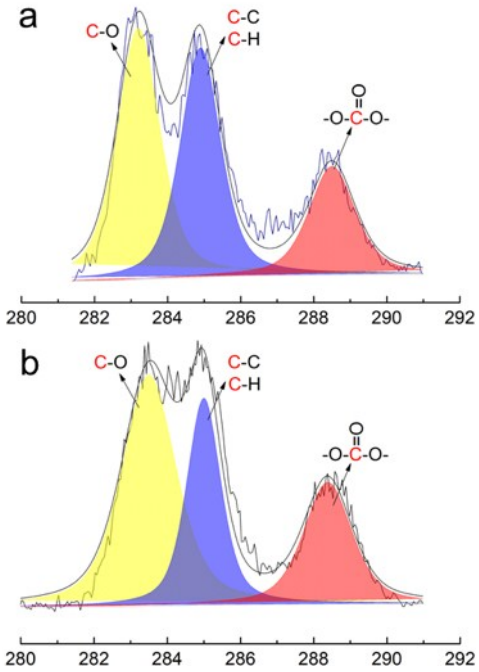

Figure S 12: High resolution C 1s XPS spectra for (a) Ag-doped Li electrodes and (b) pristine Li electrodes after 200 cycles.

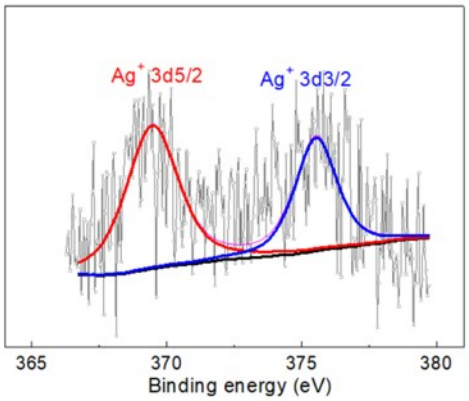

Figure S 13: High resolution Ag 3d XPS spectrum of Ag-doped Li electrodes after 200 cycles in carbonate electrolytes.

References

1. Kresse, G.; Furthmuller, J., Efficient iterative schemes for ab initio total-energy calculations using a plane-wave basis set. *Physical Review B* **1996,** *54* (16), 11169-11186.
2. Perdew, J. P.; Burke, K.; Ernzerhof, M., Generalized gradient approximation made simple. *Physical Review Letters* **1996,** *77* (18), 3865-3868.

3. Sanville, E.; Kenny, S. D.; Smith, R.; Henkelman, G., Improved grid-based algorithm for Bader charge allocation. *Journal of computational chemistry* **2007,** *28* (5), 899-908.